Physico-chemical characterization of a highly rigid Gd(III) complex formed with phenanthroline derivative ligand

Balázs Váradi,[§#] Norbert Lihi,[†] Szilvia Bunda,[§] Antónia Nagy,[§] Gréta Simon,[§] Mónika Kéri,[§] Gábor Papp,[§] Gyula Tircsó,[§] David Esteban-Gómez,[‡] Carlos Platas-Iglesias,[‡] Ferenc K. Kálmán*[§]*

[§]Department of Physical Chemistry, Faculty of Science and Technology, University of Debrecen, H-4032 Debrecen, Hungary

[#]Doctoral School of Chemistry, Faculty of Science and Technology, University of Debrecen, Egyetem tér 1, H-4032 Debrecen, Hungary

[†]ELKH-DE Mechanisms of Complex Homogeneous and Heterogeneous Chemical Reactions Research Group, Department of Inorganic and Analytical Chemistry, Faculty of Science and Technology, University of Debrecen, H-4032 Debrecen, Hungary

[‡]Centro de Investigacións Científicas Avanzadas (CICA) and Departamento de Química, Facultade de Ciencias, Univer-sidade da Coruña, 15071 A Coruña, Galicia, Spain

ABSTRACT

The discovery of the nephrogenic systemic fibrosis (NSF) and its link with the *in vivo* dissociation of certain Gd(III)-based contrast agents (CAs) applied in the magnetic resonance imaging (MRI), induced a still growing research to replace the compromised agents with safer alternatives. In the recent years several ligands were designed to exploit the luminescence properties of the lanthanides, containing structurally constrained aromatic moieties, which may form rigid Gd(III) complexes. One of these ligands is (1,10-phenanthroline-2,9-diyl)bis(methyliminodiacetic acid) (H_4FENTA) designed and synthesized for to sensitize Eu(III) and Tb(III) luminescence. Our results show that the conditional stability of the $[Gd(FENTA)]^{-}$ chelate calculated for physiological pH (pGd=19.7) is similar to those determined for $[Gd(DTPA)]^{2-}$ (pGd=19.4) and $[Gd(DOTA)]^{-}$ (pGd=20.1), routinely used in the clinical practice. The $[Gd(FENTA)]^{-}$ complex is remarkably inert with respect to its dissociation ($t_{1/2}$=872 d at pH = 7 and 25 °C), furthermore its relaxivity values determined at different field strengths and temperatures (e. g. r_{1p}=4.3 $mM^{-1}s^{-1}$at 60 MHz and 37 °C) are *ca.* one unit higher than those of $[Gd(DTPA)]^{2-}$ (r_{1p}=3.4 $mM^{-1}s^{-1}$) and $[Gd(DOTA)]^{-}$ (r_{1p}=3.1 $mM^{-1}s^{-1}$) under the same conditions. Moreover, significant improvement on the relaxivity was observed in the presence of serum proteins (r_{1p}=6.9 $mM^{-1}s^{-1}$ at 60 MHz and 37 °C). The luminescence lifetimes recorded in H_2O and D_2O solutions indicate the presence of a water molecule (q=1) in the inner sphere of the complex directly coordinated to the metal ion, possessing a relatively high water exchange rate (k_{ex}^{298}=29(2)×10^6 s^{-1}). The acceleration of the water exchange can be explained by the steric compression around the water binding site due to the rigid structure of the complex, which was supported by DFT calculations. On the basis of these results, ligands containing a phenanthroline platform have great potential in the design of safer Gd(III) agents for MRI.

Introduction

The non-invasive, high-precision diagnostic methods have become an essential part of modern medicine since the X-rays were first used under clinical conditions in 1896.[1] Over the last 100 years, the tools of medical diagnostics have been enriched by techniques such as magnetic resonance imaging (MRI), positron emission tomography (PET), single photon emission computed tomography (SPECT) or computed tomography (CT), and their combined versions.[2,3] From these techniques, MRI unambiguously provides some of the most detailed anatomical images even without the application of the so-called contrast agents (CAs), which are administered intravenously. However, in several cases the use of these agents is essential in order to visualize certain lesions.[4] Since MRI is based on the phenomenon of nuclear magnetic resonance (NMR), paramagnetic compounds are used as relaxation agents for ^{1}H nuclei (mostly water protons) located in different tissues of the human body.[3,5] Nowadays, the CAs used in clinical practice are the complexes of paramagnetic Gd(III) ion formed with polyamino-polycarboxylate ligands such as the derivatives of H_5DTPA (diethylenetriaminepentaacetic acid) and H_4DOTA (1,4,7,10-tetraazacyclododecane-1,4,7,10-tetraacetic acid).[3] Furthermore, new alternatives such as Gadopiclenol (2,2',2”-(3,6,9-triaza-1(2,6)-pyridinacyclodecaphane-3,6,9-triyl)tris(5-((2,3-dihyd-roxypropyl)amino)-5-oxopentanoic acid)), which contains a pyclen platform (3,6,9,15-tetraazabicyclo(9.3.1)pentadeca-1(15),11,13-triene) (Scheme S1), show promise in MRI investigations due to its higher relaxivity (r_1, the relaxation enhancement effect of the paramagnetic compound at 1.0 mM concentration), which allows to reduce the quantity of the CA required for a beneficial diagnosis.[6]

The *in vivo* application of the toxic Gd(III) ion (LD_{50} = 0.1-0.3 mmol/kg) ion was facilitated by the formation of thermodynamically stable and inert complexes which were considered to be

safe for years until the appearance of nephrogenic systemic fibrosis (NSF).[7,8] This potentially lethal disease was mostly reported for patients having severe renal failure when the urine excretion is slower or stopped, thereby increasing the *in vivo* life-time of the CAs increases significantly.[9,10] In this condition, the injected agent can be efficiently attacked by the endogenous metal ions and/or bioligands promoting its dechelation, which leads to the liberation and accumulation of the free Gd(III) in different tissues/organs.

Due to the "NSF-problem", concerns have been raised over the safety of contrast-enhanced MRI investigations, which prompted researchers to find alternatives for the compromised CAs.[11] A straight forward solution to this problem is to prevent the *in vivo* dechelation of the Gd(III) complexes by increasing their inertness through rigidification of the ligand skeleton.[12–14] On the other hand, paramagnetic metal ions that are essential for living systems, such as Mn(II) or Fe(III), offer a possibility of development so called biocompatible CAs reducing the risk of serious intoxication.[15–18] Albeit, whichever path is taken, many research efforts need to be devoted to design and synthesize of new paramagnetic metal complexes possessing substantial differences in their coordination-chemical properties for potential clinical use.[5]

It has been shown in the literature that rigidification of the chelators is the incorporation of aliphatic or aromatic rings into their structure, providing a rigid coordination cavity in which internal motion is extremely limited, hindering decomplexation of the chelate.[12,19–21] A remarkable example of this approach is the Gd(III) complex of the H_4CDTA (*trans*-1,2-diaminocyclohexane-*N*,*N*,*N′*,*N′*-tetraacetic acid) ligand, the cyclohexyl derivative of H_4EDTA (ethylenediaminetetraacetic acid), whose k_1 rate constant characterizing the proton-assisted dissociation is nearly 60 times smaller than that obtained for the parent chelate.[22,23] Similar results were reported recently for the Mn(II) complexes of H_4EDTA, H_4CDTA and H_4PhDTA (o-

phenylenediamine-*N*,*N*,*N*',*N*'-tetraacetic acid, Scheme S1) as evidenced by the increase of their dissociation half-lives ($t_{1/2}$) calculated for physiological pH and 25 °C, are 0.076, 12.3 and 19.1 h, respectively.[24]

Interestingly, the utilization of another important feature of the lanthanides, i.e. their luminescence, promoted the design and synthesis of several structurally rigid chelators by incorporating aromatic sensitizing moieties into the ligand structure.[25] A representative example is H_4FENTA or BBCAP (1,10-phenanthroline-2,9-diyl)bis(methyliminodiacetic acid, Scheme 1) first synthesized by Mukkala and coworkers[26] for exploiting the luminescence properties of Eu(III) and Tb(III). Furthermore, the $[Tb(FENTA)]^-$ complex was also studied by Lin and coworkers for the same reason.[27] In spite of the promising features of the luminescent $[Ln(FENTA)]^-$ complexes, to the best of our knowledge the Gd(III) complex of the H_4FENTA ligand was never explored as potential candidate for its application as MRI CA. Since this phenanthroline derivative provides a rigid and planar backbone, it is reasonable to assume that its Gd(III) complex may exhibit advantageous physico-chemical features for potential application as CAs in clinical practice. The H_4FENTA ligand can be envisioned as a rigidified derivative of H_4EGTA, (ethylene glycol-bis(2-aminoethylether)-*N,N,N′,N′*-tetraacetic acid), which was investigated extensively for lanthanide(III) complexation.[28–31] Rigidified H_4EGTA derivatives incorporating aromatic spacers and ether donor atoms have been reported.[32–35] However, since the ether oxygen donors of H_4EGTA are replaced by the nitrogen atoms of phenanthroline in H_4FENTA, the similarity between the two ligands is limited to the position and the number of the donor atoms. Even if the basicity of the aromatic nitrogen atoms are lower (pK_1=4.94 and pK_2=1.69 in 0.3 M NaCl)[36] than that of the tertiary amines of H_5DTPA or H_4DOTA, yet they can form a much stronger coordination bonds than the ether oxygen donors.

In this paper, we present the results of the thermodynamic, kinetic, relaxation, and structural study performed on the Gd(III) complex of the H_4FENTA ligand and the results were compared to those obtained for the Gd(III) complexes of H_4EGTA, H_5DTPA and H_4DOTA ligands. The structure of $[Gd(FENTA)]^-$ was accessed by DFT calculations with an aim of rationalizing the obtained physico-chemical data. The structural study was further aided by luminescence measurements performed on the Eu(III) and Tb(III) complexes and NMR studies on the Y(III) and Yb(III) analogues.

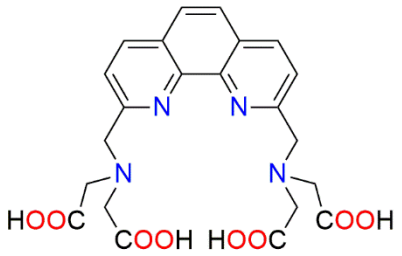

H_4FENTA

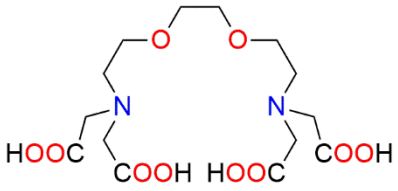

H_4EGTA

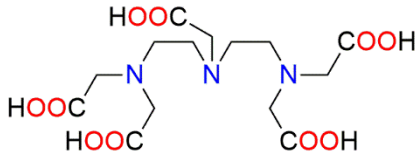

H_5DTPA

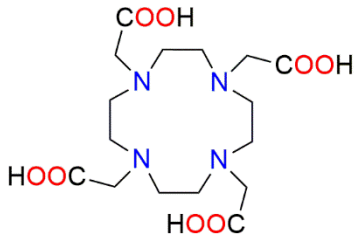

H_4DOTA

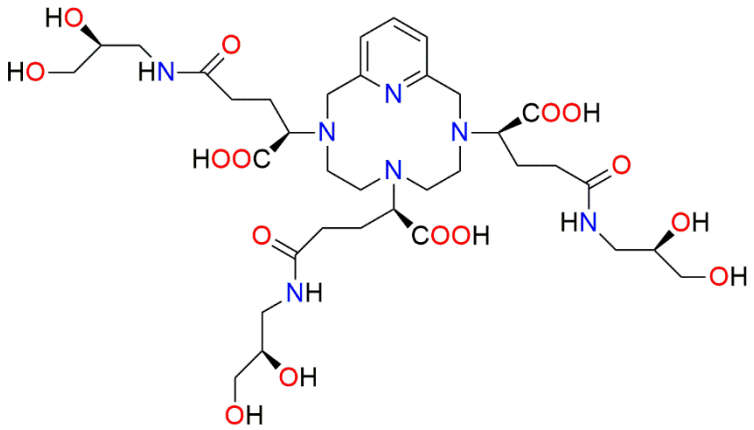

2,2',2"-(3,6,9-triaza-1(2,6)-pyridinacyclodecaphane-3,6,9-triyl)tris(5-((2,3-dihydroxypropyl)amino)-5-oxopentanoic acid), the ligand of Gadopiclenol

Scheme 1. Schematic structure of H_4FENTA and other ligands discussed in this work.

Results and discussion

Synthesis. The synthesis of the H_4FENTA ligand was performed according to the method published by Lin and coworkers.[27] The ^{1}H, ^{13}C, COSY and NOESY NMR spectra, the HPLC

chromatogram as well as the ESI-MS spectrum of the ligand confirmed the identity and purity of the chelator (Supporting Information, Figures S1-S5).

Thermodynamic and kinetic studies. First, the solution equilibria of the H_4FENTA ligand were studied with pH-potentiometric titration in the presence of NaCl (I=0.15 M, at 25 °C) to mimic the ionic strength present *in vivo*. The protonation constants of the ligand as well as the stability and protonation constants of its Gd(III) complex were determined by direct pH-potentiometric titrations. The fitting of the V(ml)-pH data pairs showed that the complexation of the Gd(III) is almost 100% at pH=2, therefore pH-potentiometry was further supported by pH-dependent relaxometric measurements. The primary data collected by the two methods were fitted together to evaluate the equilibrium constants by using the designated computational program PSEQUAD.[37] Since, the formation of the $[Gd(FENTA)]^-$ complex occurs in the acid concentration range 0.01-0.1 M, 6 batch samples containing the complex in 1 mM concentration were prepared and the $1/T_1$ and $1/T_2$ relaxation rates of the samples were measured at 60 MHz after 1 day equilibration time. The protonation and stability constants of the H_4FENTA ligand and its Gd(III) chelate were defined by Equations 1-3 (the square brackets in the equations related to the equilibrium concentrations of the species).

$$K_i^H = \frac{[H_iL]}{[H^+][H_{i-1}L]} \qquad i=1\text{-}5 \tag{1}$$

$$K_{Gd(FENTA)} = \frac{[Gd(FENTA)]^-}{[Gd(III)][FENTA]^{4-}} \tag{2}$$

$$K^H_{Gd(FENTA)} = \frac{[Gd(HFENTA]}{[Gd(FENTA)^-][H^+]} \tag{3}$$

The calculated constants are summarized in Table 1, along with the corresponding values reported for H_5DTPA and H_4DOTA complexes. Five protonation constants can be estimated for the $FENTA^{4-}$ ligand in agreement with the expected number of acid-base processes. Based on the study performed by Ryo and coworkers[38] on the protonation equilibrium of 2,9-dimethyl-1,10-phenanthroline (pK_1=5.82, pK_2=2.17, 0.3 M NaCl, 25 °C), it is reasonable to assume that the first two p*K*a values of $FENTA^{4-}$ are due to the protonation of the nitrogen atom in iminodiacetic acid moieties, because of the low basicity of the aromatic N donor atoms is expected to be lower. The remaining protonation constants are related to the protonation of either the aromatic nitrogen atoms or to the acetate pendant arms.

Table 1. The protonation constants ($\log K_i$) of the H_4FENTA ligand and protonation ($\log K_{Gd}^{H}$) and stability constants ($\log K_{Gd}$) of its Gd(III) complex.[a]

	H_4FENTA	H_4EGTA^b	H_5DTPA^c	H_4DOTA^d
$\log K_1$	8.30(3)	9.43	9.93	11.08
$\log K_2$	7.41(2)	8.82	8.37	9.23
$\log K_3$	3.52(4)	2.77	4.18	4.24
$\log K_4$	2.98(3)	2.06	2.71	4.18
$\log K_5$	2.07(4)	1.88	2.00	1.88
$\Sigma \log K_2$	*15.71*	*18.25*	*18.30*	*20.31*
$\log K_{Gd}$	19.94(6)	17.66	22.03	24.7[e]
$\log K_{Gd}^{H}$	2.74(1)	1.89	1.96	–
pGd[e]	**19.7**	**15.1**	**19.4**	**20.1**

[a] 3σ standard deviations are indicated in parenthesis. I = 0.15 M NaCl, T = 298 K. [b] Ref. [39] 0.1 M KCl, [c] Ref.[40], [d] Ref.[41] $\log K_6^{H}$=1.71 (1.0 M NaCl), [e] Ref.[42] 0.1 M NaCl, [e] Ref.[43] pGd = – $\log[Gd^{3+}_{free}]$ at c_L = 10 μM, c_{Gd} = 1 μM and pH 7.4.

The basicity of the ligands is usually estimated as the sum of the pK_a values characterizing the protonation of the donor atoms located at the ligand backbone, which have essential effect on the formation of the inner sphere complex. However, this is not always obvious, as for instance the third protonation of $DTPA^{5-}$ occurs at the central N atom forming a hydrogen bond with the central carboxylate group on the basis of the results published by Manning and Gravely.[44] On the contrary, the third protonation of the $DOTA^{4-}$ is attributed to one of the acetate moieties due to the electrostatic repulsion of the two protonated ring nitrogen atoms.[41] Therefore, only the first two pK_as of the ligands ($\Sigma\log K_2$) were considered to compare the basicity of the FENTA ligand with further Gd(III) chelators. The basicity of the H_4FENTA ligand estimated from the $\Sigma\log K_2$ values is more than 2 orders of magnitude lower than those of the reference chelators considered here.

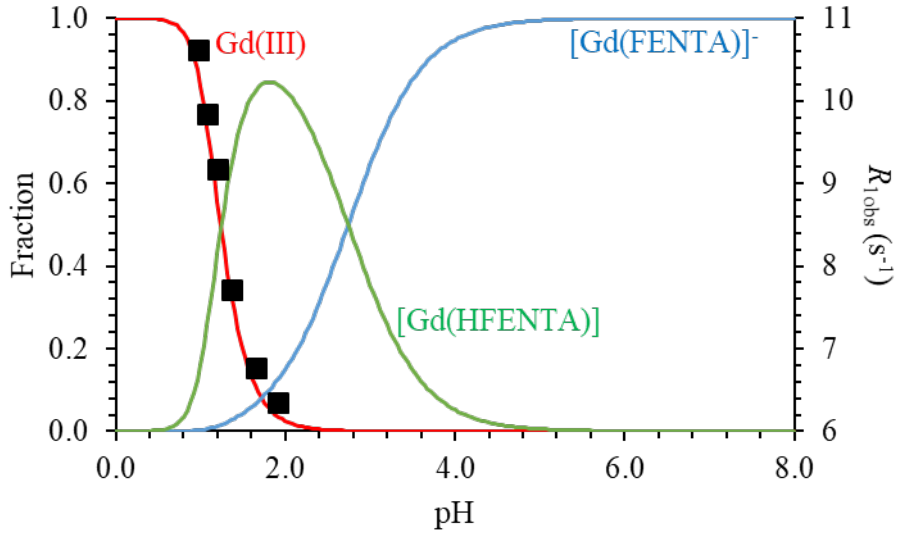

Figure 1. Concentration distribution of the complexes formed between Gd(III) and $FENTA^{4-}$, along with the $1/T_1$ relaxivity values determined by using the batch samples ($c_{Gd(III)}$=1.041 mM, c_{FENTA}=1.145 mM, I=0.15 M NaCl, T = 25 °C, 1.41 T).

The stability constant of the Gd(III) complex was determined using the relaxometric method, which involves the recording of longitudinal relaxation times of the bulk water signal at different pH values. Complex dissociation causes an increase in the relaxation rate (R_1).[45] In the fitting process, the standard deviation for the constants and the fitting parameter decreased significantly when the formation of a protonated species ([Gd(HFENTA)]) was considered. (The relaxivity values for the Gd(III) ion (r_{1p}=11.1 $mM^{-1}s^{-1}$ and r_{2p}=12.6 $mM^{-1}s^{-1}$) and for the $[Gd(FENTA)]^-$ complex (r_{1p}=5.56 $mM^{-1}s^{-1}$ and r_{2p}=6.60 $mM^{-1}s^{-1}$) were fixed while the longitudinal and transverse relaxivity of the [Gd(HFENTA)] species were calculated (r_{1p}=6.11 $mM^{-1}s^{-1}$ and r_{2p}=6.80 $mM^{-1}s^{-1}$) in the fitting procedure.) For this reason, the equilibrium data collected in the pH-potentiometric and relaxometric measurements were fitted simultaneously by assuming the existence of [Gd(HFENTA)]. The estimated equilibrium constants were used to calculate the concentration distribution diagram for the Gd(III)-H_4FENTA system that is shown in Figure 1. This equilibrium model confirms that the complex formation is almost complete near pH=2. The stability constant determined for $[Gd(FENTA)]^-$ ($\log K_{[Gd(FENTA)]^-}$=19.94(6)) is roughly two log K units higher than that determined for the complex formed with the flexible H_4EGTA ligand, though ~ two log K units lower than that of $[Gd(DTPA)]^{2-}$. Thus, the combined effect of the replacement of ether oxygen atoms in H_4EGTA with the (stronger) N donor atoms of phenanthroline and of the rigidity of the tricyclic aromatic system appear to have a beneficial effect on the thermodynamic stability of the corresponding Gd(III) complex. An empirical correlation developed recently to predict the stability of Gd(III) complexes (using structural descriptors)[46] yields estimated log$K$ values of 18.3, 17.9 and 22.3 for the complexes of $FENTA^{4-}$, $EGTA^{4-}$ and $DTPA^{5-}$, respectively. The values estimated for $[Gd(EGTA)]^-$ and $[Gd(DTPA)]^{2-}$ are in excellent agreement with those determined experimentally, while the experimental stability constant

obtained for the complex with $[Gd(FENTA)]^{-}$ is 1.6 log *K* units higher than that predicted by the empirical correlation. This likely reflects a certain ligand pre-organization associated with the presence of a rigid phenantroline unit, which contributes to an increased complex stability. DFT studies were further corroborated this statement (*vide infra*).

It needs to be emphasized that the direct comparison of the stability constants of Gd(III) complexes formed with different ligands can lead easily to misleading conclusions since the deviation in ligand basicity results in different conditional stabilities close to physiological pH. Therefore, pGd values (can be handled as conditional stability) have been calculated for the complexes by using the conditions proposed by Raymond and coworkers,[43] and listed in Table 1. These values clearly show that the stability of $[Gd(FENTA)]^{-}$ close to physiological pH does not differ significantly from that of $[Gd(DTPA)]^{2-}$ and $[Gd(DOTA)]^{-}$ but displays a considerable increase (by far more than 4 orders of magnitude) when compared to $[Gd(EGTA)]^{-}$. Consequently, the $FENTA^{4-}$ ligand exhibits excellent Gd(III) binding ability with respect to thermodynamic point.

To study the inertness of the $[Gd(FENTA)]^{-}$ complex, metal exchange reactions were carried out in the pH range between 2.4 to 4 in the presence of 20-fold Lu(III) excess applied as a scavenger for the ligand (under these conditions the displacement of the Gd(III) is quantitative). The progress of the exchange reactions was followed by ^{1}H relaxometry. Due to the high excess of the Lu(III) ion, the exchange reactions were studied under pseudo-first order conditions, thus the k_{obs} values characterizing the rate of the exchange reactions are pseudo-first order rate constants expressed as follows (Equation 4):

$$-\frac{d[Gd(FENTA)^{-}]_t}{dt} = k_{obs}[Gd(FENTA)]_t \qquad (4)$$

where $[Gd(FENTA)]_t$ is the total concentration of the complex.

The dissociation of the Gd(III) complexes may occur not only through a proton-assisted pathway but the dissociation of certain chelates (especially those formed by linear/open-chain ligands) can be enhanced by the efficient attack of exchanging metal ion via the formation of a dinuclear intermediate (as it was evidenced for $[Gd(DTPA)]^{2-}$).[47] For this reason, exchange reactions were also performed in the presence of 40-fold excess of Lu(III) at 3 different pH values (Figure 2).

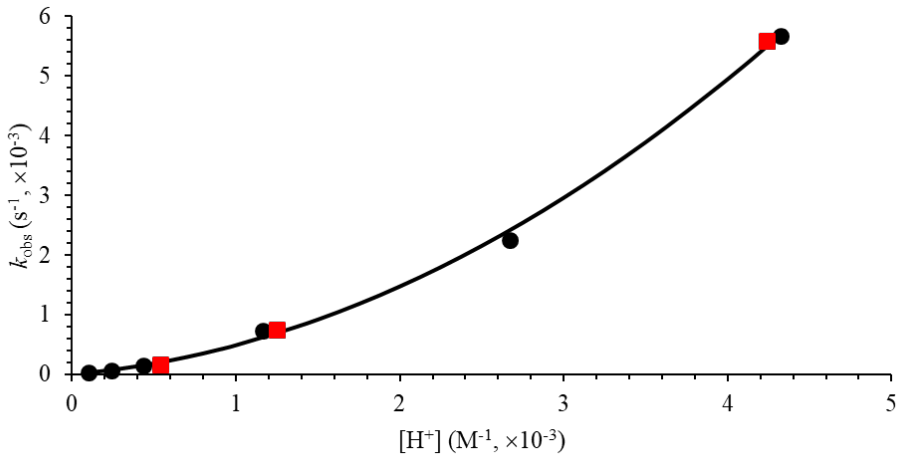

Figure 2. Dependence of the pseudo-first-order rate constants (k_{obs}) on $[H^+]$ for the $[Gd(FENTA)]^-$ complex at 10- (●) and 40-fold (■) excess of Lu(III). The lines correspond to the best fit of the k_{obs} values.

As it shown in Figure 2, the pseudo-first order rate constants increase by increasing the H^+ concentration. However, k_{obs} values obtained at different Lu(III) concentrations do not differ

within the experimental error limits. This indicates that the rate of the exchange reaction does not depend on the concentration of Lu(III), at least it does not have significant effect on the dissociation under these experimental conditions. Furthermore, the k_{obs} values exhibit a second-order dependence on $[H^+]$, which can be expressed as follows (Equation 5):

$$k_{obs} = k_0 + k_1[H^+] + k_2[H^+]^2 \quad (5)$$

However, Equation 5 was further simplified in the fitting process since the data could be satisfactorily fitted by using k_1 and k_2 rate constants only (the value of k_0 was negative value with large uncertainty). This indicates that the spontaneous dissociation (k_0) plays a negligible role in the dissociation of the complex under these experimental conditions applied. The rate constants of the proton-assisted pathways are presented in Table 2, where some data are also shown for the similar exchange reactions of $[Gd(DTPA)]^{2-}$, $[Gd(EGTA)]^-$ and $[Gd(DOTA)]^-$.

Table 2. Rate constants for the dissociation reactions of $[Gd(FENTA)]^-$, $[Gd(EGTA)]^-$, $[Gd(DTPA)]^{2-}$ and $[Gd(DOTA)]^-$ and their half-lives calculated at pH=7.4 (25 °C)

	$[Gd(FENTA)]^-$	$[Gd(EGTA)]^-$	$[Gd(DTPA)]^{2-}$ [a]	$[Gd(DOTA)]^-$ [b]
k_1 ($M^{-1}s^{-1}$)	0.23(2)	60	0.58	8.4×10^{-6}
k_2 ($M^{-2}s^{-1}$)	250(28)	–	9.7×10^4	–
$t_{1/2}$ (d) [c]	872	3.4	202	2.4×10^7

[a] Ref.[47]; [b] Ref.[48]; [c] $t_{1/2}=\ln2/k_{calc}$, pH=7.4

The values of the rate constants presented in Table 2 allow us to conclude that the proton-assisted dissociation of the linear Gd(III) complexes is much faster than that of $[Gd(DOTA)]^-$. This phenomenon originates from the more rigid coordination cavity of the macrocyclic H_4DOTA ligand. The proton-assisted dissociation occurs through the formation of a protonated intermediate complex, in which the proton has to be transferred from the oxygen donor atom of the pendant arm

to a nitrogen atom of the ligand backbone as the first step of the dissociation. This process is obviously faster when the structure of the coordination cavity is less rigid. This difference is also reflected in the half-life ($t_{1/2}$) values of dechelation calculated at physiological pH (Table 2). Furthermore, it is clear that the inertness of the $[Gd(FENTA)]^{-}$ complex is higher than that of $[Gd(DTPA)]^{2-}$, and particularly $[Gd(EGTA)]^{-}$, due to the rigid phenanthroline backbone, thereby making it as a favorable platform for the design of new CA candidates.

Photophysical properties. Luminescence lifetime measurements were recorded in solutions of the Eu(III) and Tb(III) complexes of H_4FENTA in H_2O and D_2O to determine the number of water molecules coordinated to the metal ions.[49] The two complexes can be efficiently sensitized by excitation in the absorption band of the phenanthroline unit at 278 nm (Figure 3, S6 and S7).[50] The very good match between absorption spectra and the excitation spectra recorded upon metal centered emission confirm a rather efficient ligand-to-metal energy transfer in the two complexes. The emission profile of the Eu(III) complex displays the expected $^5D_0 \rightarrow {}^7F_J$ transitions, among which the $^5D_0 \rightarrow {}^7F_2$ transition shows the highest relative intensity (52% of the overall emission intensity). This feature, together with the presence of a relatively intense $^5D_0 \rightarrow {}^7F_0$ transition, is compatible with a low symmetry of the metal coordination environment.[51] The lifetime of the $^5D_0$ excited state of Eu(III) recorded in buffered aqueous solution (0.1 M TRIS, pH 7.4) (577 μs, Table 3) is typical of monohydrated Eu(III) complexes.[52–54] The emission lifetimes recorded in H_2O and D_2O solutions afford hydration numbers of 1.2 and 1.1 using the expressions proposed by Beeby[55] and Horrocks,[49] which points to the presence of a water molecule in the first coordination sphere of the metal ion.

The emission spectrum of the Tb(III) complex displays the expected $^5D_4 \rightarrow {}^7F_J$ transitions (Figure 3). The lifetimes of the $^5D_4$ excited state provide a *q* value of 1.3,[55] confirming the results obtained for Eu(III). The quantum yields of the Eu(III) and Tb(III)-centered emission were determined using the corresponding tris(dipicolinate) complexes as standards (Table 3).[56] The quantum yield of the Eu(III) complex was found to be modest (7%), which in part is related to the quenching effect caused by the presence of a coordinated water molecule. The Tb(III) complex however presents a rather high quantum yield (32%), though quantum yields > 60% were reported for some Tb(III) derivatives.[57,58] The quenching effect of the coordinated water molecule in the $[Ln(FENTA)]^-$ complexes is likely limiting the efficiency of luminescence emission. The luminescence measurements on the $[Ln(FENTA)]^-$ (Ln = Eu or Tb) complexes confirmed the presence of coordinated water molecule in the first coordination sphere of the metal ions, thus the similar scenario is expected for the $[Gd(FENTA)]^-$ complex.

Table 3. Photophysical properties of the $[Ln(FENTA)]^-$ complexes (Ln = Eu or Tb) (0.1 M TRIS, 25 °C).

	Eu(III)	Tb
λ / nm (ε / M^{-1} cm^{-1})	279 (12 300)	278 (12 300)
τ_{H_2O} / ms	0.577	0.916
τ_{D_2O} / ms	2.218	1.306
q	1.2[a] / 1.1[b]	1.3[a]
ϕ / %	7.0	32

[a] Ref.[55], [b] Ref.[49]

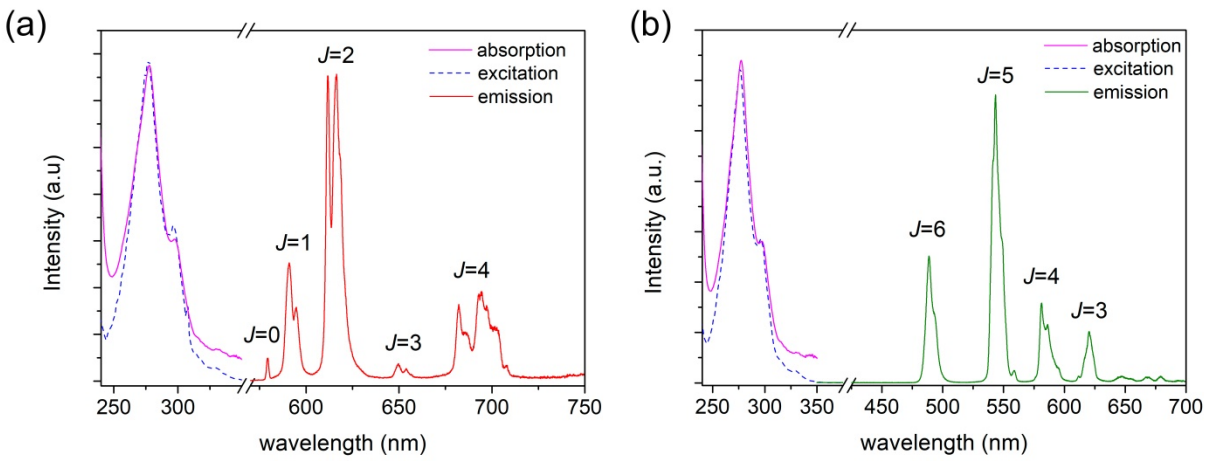

Figure 3. Absorption, excitation (λ_{em} = 613 and 545 nm for Eu(III) and Tb(III), respectively) and emission (λ_{ex} = 279 nm, excitation and emission slits 1 nm, 1×10^{-5} M, pH 7.0, 0.1 M TRIS buffer).

DFT calculations. In order to gain insight into the structure of $[Gd(FENTA)]^{-}$ complex in solution, DFT calculations were carried out. On the basis of previous literature studies,[59,60] the geometry of the complex was optimized by considering two explicit second-sphere water molecules, while the effects of the bulk solvent were introduced by use of the polarized continuum model (PCM). Details on the calculations are summarized in the Experimental section. The calculated structure is shown in Figure 4 and the corresponding Cartesian coordinates are reported in the Supporting Information (Table S1). DFT calculations predicted a distorted tricapped trigonal prism coordination polyhedron for Gd(III). The ligand binds the metal center in an octadentate coordination manner, with an inner-sphere water molecule completing coordination number nine. DFT predicted similar Gd-$N_{phenanthroline}$ distances (2.64 and 2.67 Å) and bite-angle of the phenanthroline moiety (61.2°) than those reported for the bis(phenanthroline)-gadolinium(III) complex (2.60 and 2.57 Å and 63.5°).[61] The Gd-N_{amine} distances are calculated to be 2.67 and 2.73

Å, which are shorter than those of highly rigid open-chain gadolinium(III) complexes possessing cyclobutene ring in the ligand backbone.[62] Thus, it is reasonable to assume that the rigid phenanthroline backbone pre-organizes the coordination cavity, and as a result enhances the inertness of the complex.

The distance between the Gd^{3+} and coordinated water molecule is 2.45 Å, which falls into the range of first coordination shell of water.[63] This water molecule is stabilized by two explicit water molecules through hydrogen bond network that further involves the acetate pendant arms of the ligand. This region of the complex exhibits more hydrophilic character, while obviously, the phenanthroline backbone defines a more hydrophobic region, as it is shown in the electrostatic potential surface (Figure S8). Finally, DFT calculations supported the results of luminescence measurements and predicted the presence of coordinated water molecule in the first coordination sphere of the Gd(III)ion.

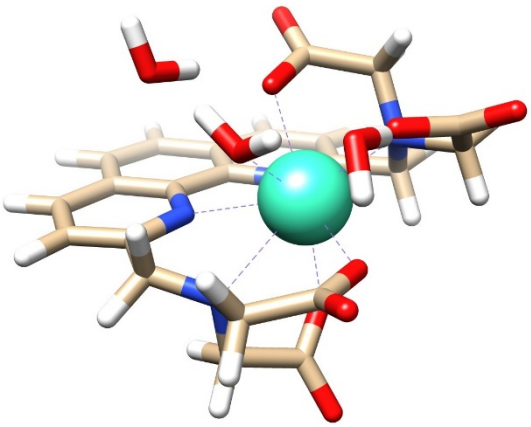

Figure 4. DFT calculated structure of the $[Gd(FENTA)(H_2O)]^-$ complex.

Relaxivity and ^{17}O NMR measurements. The relaxivity of a paramagnetic complex is one of the most important features that determines the efficacy of MRI CAs. For this reason, the

longitudinal (r_{1p}) water proton relaxation rates were estimated for $[Gd(FENTA)]^{-}$ using the relaxometric technique at 0.49 T and 1.41 T field strengths, in the presence of HEPES buffer (pK_a = 7.4, c_{HEPES} = 50 mM, I = 0.15M NaCl) to maintain pH 7, at 25 and 37 °C. The relaxivity values were obtained from the slopes of plots of $1/T_1$ versus $c_{Gd(III)}$ for 3 different concentrations (data are shown in Supporting Information, Figures S9 and S10). The results are presented in Table 4 along with the r_{1p} values obtained for $[Gd(DTPA)]^{2-}$ and $[Gd(DOTA)]^{-}$.

Table 4. The r_{1p} values ($mM^{-1}s^{-1}$) determined for the Gd(III) complexes of $FENTA^{4-}$, $DTPA^{4-}$ and $DOTA^{4-}$ ligands at pH=7.4 and 25/37 °C.

		$[Gd(FENTA)]^{-}$	$[Gd(DTPA)]^{2-}$	$[Gd(DOTA)]^{-}$
0.47 T	25 °C	5.56	4.69[a]	4.74[a]
	37 °C	4.42	3.8[b]	3.5[b]
	37 °C plasma/serum	7.79[c]	3.8[d]	4.3[d]
1.41 T	25 °C	5.36	4.24[a,e]	4.25[a,e]
	37 °C	4.03	3.4[b]	3.1[b]
	37 °C plasma/serum	6.95[c]	4.1[d]	3.6[d]

[a] Ref.[64]; [b] Ref.[65]; [c] Seronorm™ (serum), [d] Ref.[66] (plasma), [e] 50 MHz = 1.17 T, The r_{1p} values of the $[Gd(FENTA)]^{-}$ complex in serum were found to be 9.40 and 8.51 $mM^{-1}s^{-1}$ for the 0.47 and 1.41 T field strength at 25 °C, respectively.

The relaxivity of $[Gd(FENTA)]^{-}$ at both magnetic field strengths studied are higher than those reported for the Gd(III) complexes formed with $DTPA^{5-}$ and $DOTA^{4-}$ ligands used here for comparative benchmarks. These r_{1p} values are higher than those usually reported for monohydrated Gd(III) complexes. However, they agree well with the relaxivity of the rigid, monohydrated $[Gd(CBDDADPA)(H_2O)]^{-}$ complex, r_{1p} = 5.6 $mM^{-1}s^{-1}$ (Scheme S1).[62] The r_{1p}

values of [Gd(FENTA)]$^-$ decrease by increasing the temperature from 25 to 37 °C at both magnetic fields, indicating that the relaxivity is controlled by fast rotation, as it has earlier been reported for several low molecular weight Gd(III) complexes.[3] In order to get information on the relaxivity of the [Gd(FENTA)]$^-$ complex in human serum, we performed measurements for both field strengths at 25 and 37 °C. The ~50% increase in the relaxivity values indicates an interaction between the complex and the high-molar-mass proteins present in human serum. The adduct formation increases the rotational-correlation time (τ_R) of [Gd(FENTA)]$^-$, which improves significantly its relaxation enhancement effect.

The relaxivity of the Gd(III) complexes is governed by numerous microscopic parameters, one of the most important being the exchange rate of the inner sphere water molecule, k_{ex}^{298}. To gain information on the value of k_{ex}^{298}, variable temperature ^{17}O NMR measurements were performed. The obtained reduced transverse ^{17}O relaxation rates ($1/T_{2r}$) as well as chemical shifts ($\Delta\omega_r$) were used to evaluate the rate of water exchange, its activation enthalpy ($\Delta H^{\ddagger}$), the hyperfine coupling constant ($A/\hbar$) and the electronic longitudinal relaxation rates ($1/T_{1e}$) according to the Swift-Connick equations (for further details in Supporting Information), assuming a simple exponential behavior of the electron spin relaxation.[67,68] In the fitting process, the activation energy of the electron spin relaxation was kept fixed to 1 kJ/mol and the number of coordinated water molecules was set to be 1 on the basis of the relaxivity value measured at 0.49 T (r_{1p}=5.56 mM^{-1}s^{-1}) and luminescence lifetime measurements (see above). As it was demonstrated by Merbach and coworkers,[69] the temperature dependence of reduced transverse relaxation rates is actually determined by two factors, the transverse relaxation time of the bound water molecule (T_{2m}) and the mean residence time of that (τ_m) in the inner coordination sphere of Gd(III) ($1/T_{2r}$~$1/(T_{2m}+\tau_m)$). The value of T_{2m} increases with increasing temperature, while τ_m shows opposite behavior. For

$[Gd(FENTA)]^-$, the $1/T_{2r}$ values are decreasing by increasing the temperature (Figure 5), which is typical for the fast water exchange regime where $T_{2m} \gg \tau_m$.

The best-fit parameters afforded by the fitting procedure are listed in Table 5 along with the corresponding parameters determined for the Gd(III) complexes formed with the $EGTA^{4-}$, $DTPA^{5-}$ and $DOTA^{4-}$ ligands. The contribution of the electronic relaxation to the overall correlation time ($1/\tau_c = k_{ex} + 1/T_{1e}$) was also calculated in the investigated temperature range. On the basis of the calculations, the contribution of the water exchange is increasing from 37% to 93% in the temperature range 273-348 K, which ensures a rather accurate determination of k_{ex}.

The water exchange rate obtained for $[Gd(FENTA)]^-$ is relatively fast in comparison with those determined for $DOTA^{4-}$ and $DTPA^{5-}$ complexes,[70] but similar to that determined for the $EGTA^{4-}$ derivative.[30] Similarly, differences can be observed between the electronic relaxation of $[Gd(FENTA)]^-$ ($1.5(2)\times10^7$ s^{-1}) and $[Gd(DOTA)]^-$ (0.25×10^7 s^{-1}), which indicates that the different coordination environments of Gd(III) have a great impact on the electron spin relaxation. Furthermore, the acceleration of the water exchange in the case of structurally similar complexes, like $[Gd(DOTA)]^-$ and $[Gd(DODPA)]^+$, was explained by the steric compression around the water binding site.[71–73]

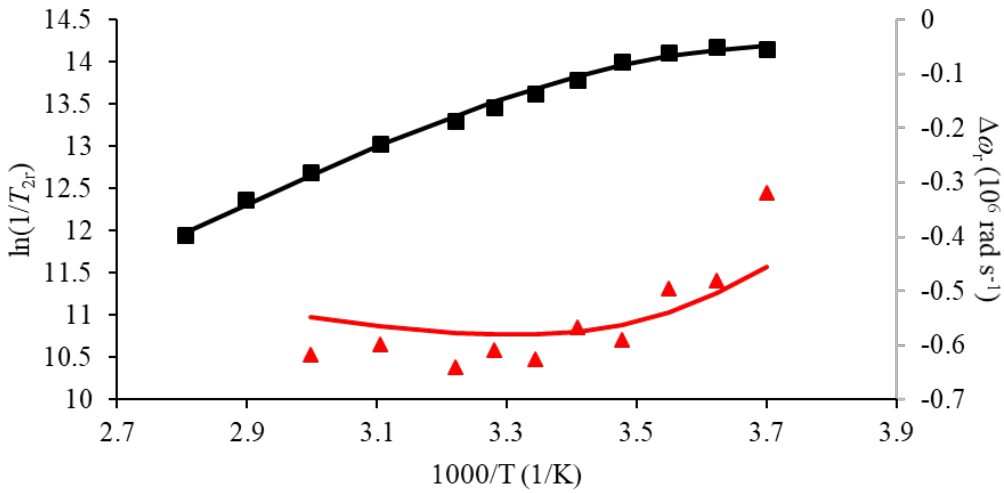

Figure 5. Reduced transverse ^{17}O relaxation rates (■) and ^{17}O chemical shifts (▲) observed for $[Gd(FENTA)]^-$ solution at 9.4 T and pH=7.4 (c_{GdL}=20 mM).

Table 5. Best-fit parameters obtained from the analysis of the reduced relaxation ^{17}O NMR rates of $[Gd(FENTA)]^-$ recorded at 9.4 T together with the corresponding values of $[Gd(DTPA)]^{2-}$ and $[Gd(DOTA)]^-$.

	$[Gd(FENTA)]^-$	$[Gd(EGTA)]^{-\,a}$	$[Gd(DTPA)]^{2-\,b}$	$[Gd(DOTA)]^{-\,b}$
k_{ex}^{298} / 10^6 s^{-1}	29(2)	31	3.3	4.1
$\Delta H^{\ddagger}$ / kJ mol^{-1}	29(1)	11	51.6	49.8
$A/\hbar$ / 10^6 rad s^{-1}	-2.77(8)	-3.2	-3.8	-3.7
$1/T_{1e}$ / 10^7 s^{-1}	1.5(2)	–	–	0.25[b]

[a] Ref. [30], [b] Ref.[64];

The hyperfine coupling constant ($A/\hbar$ = –2.77(8)×10^6 rad s^{-1}), characterizing the hyperfine interaction between the electron spin of the paramagnetic metal ion and the spin of the water ^{17}O nucleus in the inner sphere of the complex, falls slightly out from range reported for Gd(III)

complexes (–3.9±0.3×10^6 rad s^{-1}).[59] Since $A/\hbar$ is proportional to the number of the coordinated water molecule(s) (q), if the water exchange is fast enough on the NMR time scale, its lower value can indicate a q which is lower than 1 due to a possible hydration equilibrium in solution. However, this assumption is contradicted with the high relaxivity found for $[Gd(FENTA)]^-$, r_{1p}=5.56 $mM^{-1}s^{-1}$ at 0.47 T and 25 °C, and the hydration numbers obtained from luminescence measurements for the Eu(III) and Tb(III) analogues. Similarly low $A/\hbar$ values were observed for the Gd(III) complex of the linear $OCTAPA^{4-}$ ligand (-2.31×10^6 rad s^{-1})[14] and for $[Gd(DODPA)]^+$ (-2.2×10^6 rad s^{-1}),[72] which contain picolinate pendants in their structure. This observation suggests that the aromatic moieties in the ligand backbone may have an influence on the hyperfine coupling constants, likely by providing an efficient path for delocalization of spin density. Moreover, the calculated hyperfine coupling constant calculated with DFT ($A/\hbar$, –3.3×10^6 rad s^{-1}) is in reasonable agreement with the experimental value and further confirmed the hydration number of the complex.

^{1}H and ^{13}C NMR studies. In order to confirm the complex formation and support the DFT calculations in regard to the compact structure found for the Gd(III) complex, 1D and 2D NMR measurements were carried out on aqueous solutions of the ligand and the Eu(III), Yb(III) and Y(III) complexes (Figure 6-7 and Figure S11-S13). These metal ions are often used to study the binding mode in gadolinium(III) complexes because Gd(III) cannot be applied in NMR spectroscopy due to its extreme line broadening effect. The comparison of the ^{1}H NMR spectra of the H_4FENTA ligand and $[Eu(FENTA)]^-$ complex is shown in Figure 6. The paramagnetism of the metal ion induces significant paramagnetic shifts for the aromatic proton nuclei, especially those being close to the amino-carboxylate pendants. The signals corresponding to the aliphatic protons in the region 2-4 ppm are extremely broad, suggesting the presence of dynamic processes

in solution. The DFT structure obtained for this complex evidence that two acetate arms are lying close to the plane defined by the phenanthroline moiety (in-plane), while the other two are situated above and below that plane (out-of-plane). Thus, most likely the dynamic process responsible for the line-broadening of the CH_2 protons involves the exchange between in-plane and out-of-plane acetate groups, as observed previously for complexes containing an aromatic tridentate unit functionalized with iminodiacetate groups moiety.[74]

The dynamics of the complexes of H_4FENTA were also investigated using the diamagnetic Y(III) analogue. The ^{13}C NMR spectrum recorded in D_2O at high temperature shows six aromatic signals in the range 157.5 – 122.8 ppm, two well-resolved aliphatic signals at 64.1 and 63.8 ppm, and a single carbonyl signal at 179.5 ppm. This spectral pattern is consistent with a fast interconversion of the in-plane and out-of-plane acetate groups. The ^{13}C NMR signals of the carbonyl and CH_2 groups broaden below 55 ºC, while the aromatic carbon signals remain sharp (Figure S11). The carbonyl and CH_2 signals are very broad at 5 ºC, but unfortunately, the slow exchange regime could not be attained above the freezing point of the solvent.

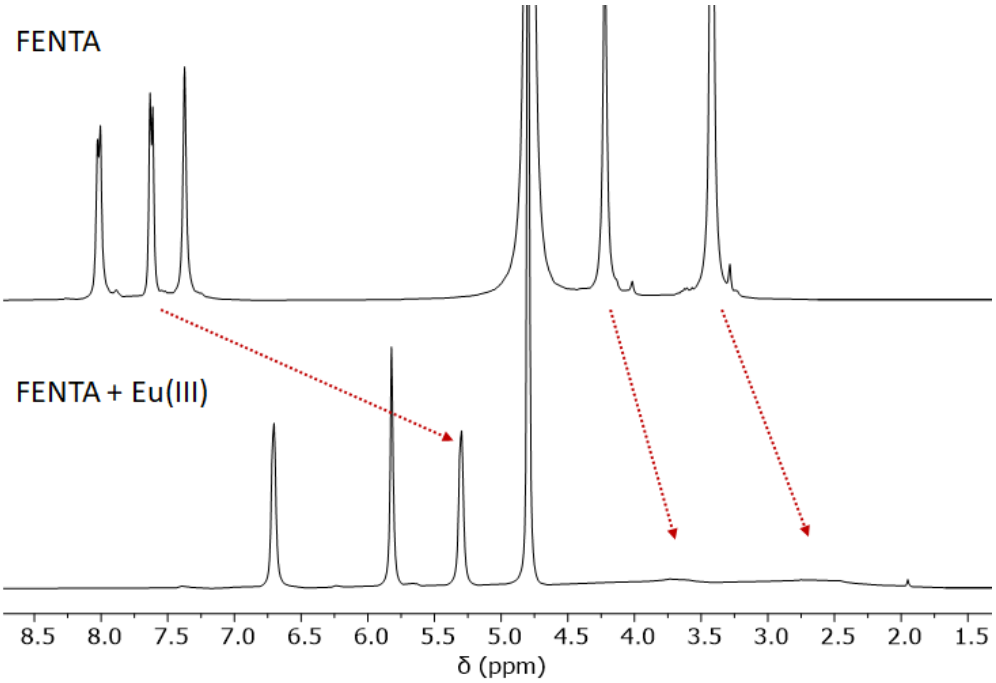

Figure 6. ^{1}H NMR spectra of H_4FENTA ligand (pH=8.9) and $[Eu(FENTA)]^{-}$ complex (pH=7.7) (D_2O, T = 298 K). The arrows highlight the coordination induced changes in the spectra.

The ^{1}H NMR spectrum of the Yb(III) analogue is better resolved, displaying nine paramagnetically shifted signals in the range ~26 to -23 ppm, which is in line with an effective C_2 symmetry of the complex in solution. The in-plane and out-of-plane acetate groups give two sets of signals, as evidenced by the presence of six signals due to CH_2 protons, indicating slow interconversion in the NMR time scale (Figure 7). We also notice the presence of a second group of paramagnetically-shifted signals that evidences the formation of a second complex species.

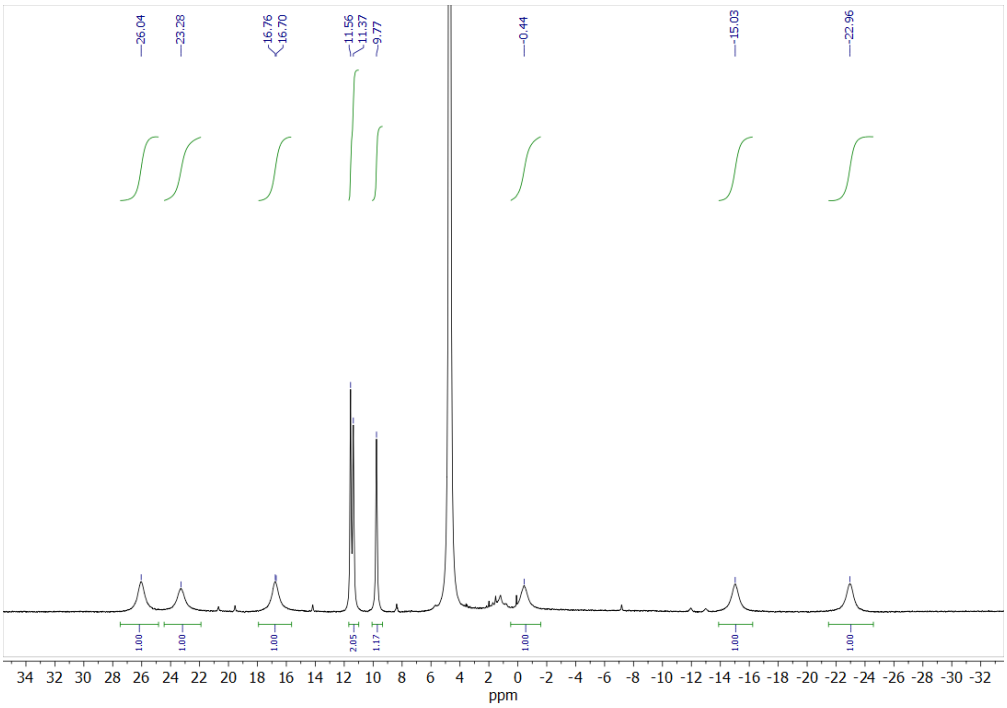

Figure 7. ^{1}H NMR spectra of [Yb(FENTA)]$^{-}$ recorded in D_2O (400 MHz, 25 ºC, pH 7.4)

Since the aromatic protons of the phenanthroline backbone are relatively far from the coordination cavity,[75] the paramagnetic effect of the Eu(III) does not cause extensive line-broadening, providing the possibility to measure the self-diffusion of the complex. The diffusion coefficient of the ligand (D = 3.45×10^{-10} m^2/s) slightly increases (D = 3.69×10^{-10} m^2/s) for [Eu(FENTA)]$^{-}$, which indicates that the hydrodynamic radius of the complex is decreased upon the coordination of the iminodiacetate arms to the metal ion, i.e. the formation of a more compact structure.[76] Similar diffusion coefficients were obtained in D_2O solution for small mononuclear lanthanide(III) complexes.[77,78] These diffusion coefficients rule out that the dynamic process evidenced by ^{1}H NMR spectra are related to intermolecular interactions (aggregation), but rather

to an intramolecular exchange process. The 2D DOSY spectra are presented in the Supporting Information (Figure S13).

Conclusions

In this work we have investigated the coordination properties towards Gd(III) and other lanthanide ions of the non-macrocyclic ligand H_4FENTA, which contains a rigid phenanthroline unit. We have shown that the rigidity imparted by the aromatic unit increases significantly the thermodynamic stability of the complex and its inertness with respect to dissociation, as evidenced by the comparison with H_4EGTA. The Gd(III) complex also displays a ^{1}H relaxivity that is somewhat higher than those of the H_5DTPA and H_4DOTA complexes. The coordinated water molecule is involved in a rather fast exchange with bulk water, as demonstrated by ^{17}O NMR measurements. ^{1}H and ^{13}C NMR spectra performed on the Eu(III) and Y(III) complexes evidence a certain fluxionality of the complexes in solution, which is associated to a flip of the acetate groups from in-plane to out-of-plane positions. Thus, even when the rigid phenanthroline unit improves the properties of the ligand for stable and inert Gd(III) complexation, further structural modifications leading to enhanced rigidity may be envisaged to obtain improved systems.

Experimental section

The metal salts and other materials used in the experiments were purchased from commercial sources and used without further purification (the purity of $LnCl_3$ salt is 99.9%). Standardized Na_2H_2EDTA was used to determine the concentration of the $LnCl_3$ solutions by complexometric titration in the presence of xylenol orange as indicator. The $[Ln(FENTA)]^-$ complexes were prepared by mixing solutions of the ligand and metal ion of known concentrations to reach a 1:1 stoichiometric ratio, followed by pH adjustment.

Equilibrium studies. The protonation constant of the H_4FENTA ligand and the protonation and stability constants of its Gd(III) complex were studied by pH-potentiometric titrations supported by relaxometric measurements. The exact ligand concentration was calculated from the potentiometric curves. For the pH-potentiometric titrations, a Metrohm 888 Titrando titration workstation and a Metrohm-6.0233.100 combined electrode were used. The electrode was calibrated by using KH-phthalate (pH=4.005) and borax (pH=9.177) buffers. The titrated samples (6.0 mL) were thermostated (25 °C) and stirred under inert (N_2) atmosphere to avoid the effect of CO_2 and O_2. The ionic strength of the samples was set to 0.15 with NaCl. The titrations were carried out by means of 0.2 M NaOH in solutions containing ligand or ligand and metal ion in 1 to 1 ratio (c_L=c_M=2 mM). During the titrations 150-200 mL–pH data pairs were recorded in the pH range of 1.8-12.0 for the ligand and 1.6-11.5 for the complex. For the calculation of [H^+] from the pH values, the Irving factor of the electrode was determined by titrating an acid (0.01 M HCl) solution with standardized NaOH.[79] The value of the ion product of water (K_w) was determined in the same titration. The equilibrium constants were evaluated by using the PSEQUAD program.[37] Because of the high stability of the Gd(III) complex (the complex formation is almost complete by pH=2), 6 out-of-cell samples in the acid concentration range 0.01-0.1 M (I=[Na^+]+[H^+]=0.15 M) were prepared and their T_1 and T_2 relaxation times were measured after 1 day equilibration time. For the relaxivity measurements Bruker Minispec MQ-60 NMR Analyzer was used (more details below).

Kinetic measurements. The rate of the metal exchange reaction taking place between the [Gd(FENTA)]$^-$ complex and the Lu(III) ion was studied at 25 °C and 0.15 M NaCl ionic strength by a Bruker Minispec MQ-60 NMR Analyzer measuring the $1/T_1$ relaxation rates of the samples in the pH range between 2.4 – 4.0. The concentration of the complex was 1 mM while the Lu(III)

ion was applied in 20-fold excess. The pH was maintained by a mixture of non-coordinating buffers, chloroacetic acid (pK_a=2.9, 50 mM) and 1,4-dimethylpiperazine (pK_a=4.2, 50 mM). In order to investigate the effect of the Lu(III) on the dissociation rate of the complex, the exchange reactions were carried out in the presence 40-fold excess of that as well at 3 different pH. The high excess of Lu(III) ensures the pseudo-first order conditions simplifying the evaluation of the kinetic data. The data fit was carried out with the program Micromath Scientist using a least-squares fitting approach. The pseudo-first-order rate constants (k_{obs}) were obtained by fitting the $1/T_1$ values measured at different times on the basis of Equation 6.

$$R_t = (R_0 - R_e)e^{-k_{obs}t} + R_e \quad (6)$$

where R_0, R_t, and R_e are the absorbance values measured at the start, at time t, and at equilibrium, respectively.

The ^{1}H longitudinal (T_1) relaxation times were measured by using Bruker Minispec MQ-20 and MQ-60 NMR Analyzers. The temperature of the sample was set to 25.0(±0.2) or 37.0(±0.2) °C. The r_{1p} values were measured by using the inversion−recovery method (180°−τ−90°) averaging 4−6 data points obtained at 10 different τ delay values. In the equilibrium measurements, the $1/T_2$ values of the batch samples were also recorded at 25.0(±0.2) °C by means of the Carl–Purcell–Meiboom–Gill (CPMG) spin-echo pulse sequence.[80] The relaxivity values were obtained from the slopes of plots $1/T_1$ versus $c_{Gd(III)}$ for 3 concentrations. The pH of the samples (0.3−0.4 ml) samples was set to 7.4 by 0.05 M HEPES buffer. The relaxivity values of the Gd(FENTA)]$^-$ complex in serum were determined by using Seronorm solution (Seronorm™ SERO = lyophilized human blood serum with no preservatives or stabilizers added). One bottle of lyophilized serum was dissolved in 4 ml of water. After the complete dissolution, 1 ml of a 5.0 mM complex solution

was added and pH was adjusted to 7.4. The relaxivity values were determined by *Bruker Minispec MQ60* relaxometer at 0.47 T and 1.41 T field strength as well as 25.0±0.2 °C and 37.0±0.2 °C.

NMR measurements. In the ^{17}O NMR experiments, the longitudinal (T_1) and transverse (T_2) relaxation times and chemical shifts of the ^{17}O nuclei in an aqueous solution of the Gd(III) complex (pH=7.4, at 20 mM concentration) and of a diamagnetic reference ($HClO_4$ acidified water, pH=3.0) were recorded in the temperature range 273−348 K by means of a Bruker Avance 400 (9.4 T, 54.2 MHz) spectrometer. The temperature was calibrated by using ethylene glycol as the standard.[81] T_1 and T_2 values were determined by the inversion−recovery and CPMG techniques, respectively.[80] In order to avoid the susceptibility corrections of the chemical shifts, a glass sphere fitted into a 10 mm NMR tube was used during the measurements.[82] The samples were enriched with ^{17}O to 2% with 10% $H_2{}^{17}O$ (NUKEM) water. The data fit was carried out with the program Micromath Scientist using a least-squares fitting procedure. ^{17}O NMR data have been fitted according to the Swift and Connick equations.[67,68] The equations in the calculation are presented in the ESI.

For high-resolutionthe NMR experiments the H_4FENTA ligand and its Eu(III) complex were dissolved in D_2O. The ^1H, ^{13}C, 2D COSY (correlation spectroscopy) and NOESY (nuclear Overhauser effect spectroscopy) NMR measurements were performed with a 360 Bruker Avance I NMR spectrometer and a 400 MHz Bruker Avance II instrument equipped with a gradient probe head. For the NOESY spectrum the mixing time was set to 800 ms. For all measurements, standard pulse sequences were used, and the temperature was kept at 298 K. The self-diffusion of the ligand was measured with PGSE (pulse gradient spin echo) pulse sequence using bipolar gradient pulses (BIPLED)[83] at a 500 MHz Bruker Avance II spectrometer equipped with a TXI probe head. The diffusion time (Δ) was set to 40 ms and a 6 ms gradient pulse length (δ) was applied, while the

gradient strength (G) was increased in 64 square distant steps. The diffusion coefficient was calibrated for HOD.[84] The spectra were post-processed with MestReNova 9.0. Diffusion coefficients (D_{obs}) were calculated according to Equation 7,[85]

$$I = I_0 \, exp(-D_{obs}\gamma^2\delta^2G^2(\Delta - \delta/3) \quad (7)$$

where I and I_0 are the measured and initial signal intensities, respectively, and γ is the gyromagnetic ratio of the proton nuclei. The fitting procedure of the exponential decays was carried out with the nonlinear least-squares method (by OriginPro 8.6© software) as well as with inverse Laplace transformation (Multi-Exponential Relaxation Analysis, MERA),[86] while the 2D DOSY transform was performed with the "peak fit" method.

Absorption and emission spectra. UV−vis spectra were recorded on a JENWAY 6850 UV-vis spectrometer using 1 and 4 mm quartz cells. Excitation and emission spectra were measured with a Horiba FluoroMax Plus-P spectrofluorometer equipped with a continuous 150 W xenon arc lamp (ozone-free), an R928P photon counting emission detector and a photodiode reference detector for monitoring lamp output. Luminescence decays were measured with a time-correlated single-photon counting system and a xenon flash lamp as light source.

DFT calculations. The ground state geometry of the $[Gd(FENTA)(H_2O)]^-$ complex was computed using the Gaussian 09 software package (ES64L-G09 RevE.01) at the DFT level of theory.[87] In this calculation, the TPSSh exchange-correlation functional[88,89] was used together with the quasi-relativistic effective core potential including 53 electrons in the core (ECP53MWB) with the corresponding (7s6p5d)/[5s4p3d] basis sets for Gd.[90,91] All other atoms (C, H, N, O) were treated with the 6-311G(d,p) basis set. The effect of the solvent was taken into account by using the integral equation formalism variant of the polarizable continuum model (IEFPCM).[92] Single-

point frequency calculations at the same level of theory were also carried out for the ground state geometry, which represented a true energy minimum (0 imaginary frequencies) on the potential energy surface. ^{17}O hyperfine coupling constant was computed through the ORCA software[93] (version 4.0.1.2). In this calculation, the SARC2-DKH-QZVP[94] basis set was used for Gd, while the other atoms were treated with the DKH-*def2*-TZVP[95,96] according to the protocol reported earlier. The resolution of identity and chain of spheres exchange (RIJCOSX) approximation[97,98] was used to accelerate the calculations with the SARC2-DKH-QZVP/JK auxiliary basis set for Gd, while the auxiliary basis set of the other atoms were generated through the AutoAux procedure.[99] The calculation included the polarizable continuum model to consider the effect of the solvent. In these calculations, tight SCF convergence criteria were employed.

ASSOCIATED CONTENT

Supporting Information. Details on the synthesis, ^{1}H, ^{13}C NMR and MS spectra of the ligand, UV-vis absorption spectra, energy and Cartesian coordinates obtained by DFT, relaxometric and NMR studies.

AUTHOR INFORMATION

Corresponding Author

*E-mail for Ferenc K. Kálmán: kalman.ferenc@science.unideb.hu

Author Contributions

The manuscript was written through contributions of all authors. All authors have given approval to the final version of the manuscript.

Notes

The authors declare no competing financial interest and there are no conflicts to declare.

ACKNOWLEDGMENT

The research was funded by the Hungarian National Research, Development and Innovation Office (PD-135169, FK-134551, K-128201, K-139140) projects, the bilateral Hungarian−Spanish Science and Technology Cooperation Program (2019-2.1.11-TET-2019-00084), the New National Excellence Program ÚNKP-21-5 (F. K. K.) and ÚNKP-21-4-II (N.L.). C.P.-I. and D. E.-G. thank Ministerio de Ciencia e Innovación (Grant PID2019-104626GB-I00) for generous financial support. F. K. K. acknowledges financial support of the János Bolyai Research Scholarship of the Hungarian Academy of Sciences. The authors are indebted to KIFÜ for awarding access to resource based in Hungary. The scientific research was supported by the Gedeon Richter's Talentum Foundation established by Gedeon Richter Plc (Gedeon Richter Ph.D. Fellowship). The research was prepared with the professional support of the Doctoral Student Scholarship Program of the Cooperative Doctoral Program of the Ministry of Innovation and Technology financed from the National Research, Development and Innovation Fund (NKFIH). Project TKP2020-NKA-04 has been implemented with support provided by the National Research, Development and Innovation Fund of Hungary, financed under the 2020-4.1.1-TKP2020 funding scheme.

REFERENCES

(1) Feldman, A. A Sketch of the Technical History of Radiology from 1896 to 1920. *RadioGraphics* **1989**, *9* (6), 1113–1128.

(2) *Imaging Modalities for Biological and Preclinical Research: A Compendium, Volume 2: Parts II–IV: In Vivo Preclinical Imaging, Multimodality Imaging and Outlook*; Walter, A., Mannheim, J. G., Caruana, C. J., Eds.; IOP Publishing, 2021.
(3) *The Chemistry of Contrast Agents in Medical Magnetic Resonance Imaging*, Second edition.; Helm, L., Merbach, A. E., Tóth, É., Eds.; John Wiley & Sons Inc: Hoboken, NJ, 2013.
(4) Cheng, W.; Ping, Y.; Zhang, Y.; Chuang, K.-H.; Liu, Y. Magnetic Resonance Imaging (MRI) Contrast Agents for Tumor Diagnosis. *Journal of Healthcare Engineering* **2013**, *4* (1), 23–46.
(5) Wahsner, J.; Gale, E. M.; Rodríguez-Rodríguez, A.; Caravan, P. Chemistry of MRI Contrast Agents: Current Challenges and New Frontiers. *Chem. Rev.* **2019**, *119* (2), 957–1057.
(6) Napolitano, R.; Lattuada, L.; Baranyai, Z.; Guidolin, N.; Marazzi, G. Gadolinium Bearing Pcta-Based Contrast Agents. WO2020030618A1, 2020.
(7) Weinmann, H.; Brasch, R.; Press, W.; Wesbey, G. Characteristics of Gadolinium-DTPA Complex: A Potential NMR Contrast Agent. *American Journal of Roentgenology* **1984**, *142* (3), 619–624.
(8) Allard, M.; Doucet, D.; Kien, P.; Bonnemain, B.; Caillé, J. M. Experimental Study of DOTA-Gadolinium Pharmacokinetics and Pharmacologic Properties: *Investigative Radiology* **1988**, *23*, S271–S274.
(9) Grobner, T. Gadolinium – a Specific Trigger for the Development of Nephrogenic Fibrosing Dermopathy and Nephrogenic Systemic Fibrosis? *Nephrology Dialysis Transplantation* **2006**, *21* (4), 1104–1108.
(10) Marckmann, P.; Skov, L.; Rossen, K.; Dupont, A.; Damholt, M. B.; Heaf, J. G.; Thomsen, H. S. Nephrogenic Systemic Fibrosis: Suspected Causative Role of Gadodiamide Used for Contrast-Enhanced Magnetic Resonance Imaging. *JASN* **2006**, *17* (9), 2359–2362.
(11) Bennett, C. L.; Qureshi, Z. P.; Sartor, A. O.; Norris, L. B.; Murday, A.; Xirasagar, S.; Thomsen, H. S. Gadolinium-Induced Nephrogenic Systemic Fibrosis: The Rise and Fall of an Iatrogenic Disease. *Clinical Kidney Journal* **2012**, *5* (1), 82–88.
(12) Tircsó, G.; Regueiro-Figueroa, M.; Nagy, V.; Garda, Z.; Garai, T.; Kálmán, F. K.; Esteban-Gómez, D.; Tóth, É.; Platas-Iglesias, C. Approaching the Kinetic Inertness of Macrocyclic Gadolinium(III)-Based MRI Contrast Agents with Highly Rigid Open-Chain Derivatives. *Chem. Eur. J.* **2016**, *22* (3), 896–901.
(13) Rodríguez-Rodríguez, A.; Regueiro-Figueroa, M.; Esteban-Gómez, D.; Tripier, R.; Tircsó, G.; Kálmán, F. K.; Bényei, A. C.; Tóth, I.; Blas, A. de; Rodríguez-Blas, T.; Platas-Iglesias, C. Complexation of Ln^{3+} Ions with Cyclam Dipicolinates: A Small Bridge That Makes Huge Differences in Structure, Equilibrium, and Kinetic Properties. *Inorg. Chem.* **2016**, *55* (5), 2227–2239.
(14) Platas-Iglesias, C.; Mato-Iglesias, M.; Djanashvili, K.; Muller, R. N.; Elst, L. V.; Peters, J. A.; de Blas, A.; Rodríguez-Blas, T. Lanthanide Chelates Containing Pyridine Units with Potential Application as Contrast Agents in Magnetic Resonance Imaging. *Chem. Eur. J.* **2004**, *10* (14), 3579–3590.
(15) Rolla, G. A.; Platas-Iglesias, C.; Botta, M.; Tei, L.; Helm, L. ^{1}H and ^{17}O NMR Relaxometric and Computational Study on Macrocyclic Mn(II) Complexes. *Inorg. Chem.* **2013**, *52* (6), 3268–3279.
(16) Garda, Z.; Molnár, E.; Kálmán, F. K.; Botár, R.; Nagy, V.; Baranyai, Z.; Brücher, E.; Kovács, Z.; Tóth, I.; Tircsó, G. Effect of the Nature of Donor Atoms on the Thermodynamic,

Kinetic and Relaxation Properties of Mn(II) Complexes Formed With Some Trisubstituted 12-Membered Macrocyclic Ligands. *Front. Chem.* **2018**, *6*, 232.

(17) Garda, Z.; Forgács, A.; Do, Q. N.; Kálmán, F. K.; Timári, S.; Baranyai, Z.; Tei, L.; Tóth, I.; Kovács, Z.; Tircsó, G. Physico-Chemical Properties of MnII Complexes Formed with Cis- and Trans-DO2A: Thermodynamic, Electrochemical and Kinetic Studies. *Journal of Inorganic Biochemistry* **2016**, *163*, 206–213.

(18) Baranyai, Z.; Carniato, F.; Nucera, A.; Horváth, D.; Tei, L.; Platas-Iglesias, C.; Botta, M. Defining the Conditions for the Development of the Emerging Class of Fe^{III} -Based MRI Contrast Agents. *Chem. Sci.* **2021**, *12* (33), 11138–11145.

(19) Molnár, E.; Camus, N.; Patinec, V.; Rolla, G. A.; Botta, M.; Tircsó, G.; Kálmán, F. K.; Fodor, T.; Tripier, R.; Platas-Iglesias, C. Picolinate-Containing Macrocyclic Mn^{2+} Complexes as Potential MRI Contrast Agents. *Inorg. Chem.* **2014**, *53* (10), 5136–5149.

(20) Kálmán, F. K.; Végh, A.; Regueiro-Figueroa, M.; Tóth, É.; Platas-Iglesias, C.; Tircsó, G. H_4 Octapa: Highly Stable Complexation of Lanthanide(III) Ions and Copper(II). *Inorg. Chem.* **2015**, *54* (5), 2345–2356.

(21) Vágner, A.; Gianolio, E.; Aime, S.; Maiocchi, A.; Tóth, I.; Baranyai, Z.; Tei, L. High Kinetic Inertness of a Bis-Hydrated Gd-Complex with a Constrained AAZTA-like Ligand. *Chem. Commun.* **2016**, *52* (75), 11235–11238.

(22) Brücher, E.; Szarvas, P. Kinetic Study of the Isotope-Exchange Reactions of the Central Ions of the Lanthanide Ethylenediaminetetraacetate and Trans-1,2-Diaminocyclohexanetetraacetate Complexes. *Inorganica Chimica Acta* **1970**, *4*, 632–636.

(23) Nyssen, G. A.; Margerum, D. W. Multidentate Ligand Kinetics. XIV. Formation and Dissociation Kinetics of Rare Earth-Cyclohexylenediaminetetraacetate Complexes. *Inorg. Chem.* **1970**, *9* (8), 1814–1820.

(24) Pota, K.; Garda, Z.; Kálmán, F. K.; Barriada, J. L.; Esteban-Gómez, D.; Platas-Iglesias, C.; Tóth, I.; Brücher, E.; Tircsó, G. Taking the next Step toward Inert Mn^{2+} Complexes of Open-Chain Ligands: The Case of the Rigid PhDTA Ligand. *New J. Chem.* **2018**, *42* (10), 8001–8011.

(25) Hasegawa, M.; Ohmagari, H.; Tanaka, H.; Machida, K. Luminescence of Lanthanide Complexes: From Fundamental to Prospective Approaches Related to Water- and Molecular- Stimuli. *Journal of Photochemistry and Photobiology C: Photochemistry Reviews* **2022**, 100484.

(26) Mukkala, V.-M.; Sund, C.; Kwiatkowski, M.; Pasanen, P.; Högberg, M.; Kankare, J.; Takalo, H. New Heteroaromatic Complexing Agents and Luminescence of Their Europium(III) and Terbium(III) Chelates. *HCA* **1992**, *75* (5), 1621–1632.

(27) Lin, P.; Zheng, H.; Zhu, Q.-Z.; Xu, J.-G. A New Fluorimetric Reagent for Highly Selective and Sensitive Determination of Terbium Ion. *Microchimica Acta* **2002**, *140* (1–2), 125–129.

(28) Tei, L.; Botta, M.; Lovazzano, C.; Barge, A.; Milone, L.; Aime, S. 1H and 17O NMR Relaxometric Study in Aqueous Solution of Gd(III) Complexes of EGTA-like Derivatives Bearing Methylenephosphonic Groups. *Magn. Reson. Chem.* **2008**, *46* (S1), S86–S93.

(29) Yerly, F.; Hardcastle, K. I.; Helm, L.; Aime, S.; Botta, M.; Merbach, A. E. Molecular Dynamics Simulation of $[Gd(Egta)(H_2O)]^-$ in Aqueous Solution: Internal Motions of the Poly(Amino Carboxylate) and Water Ligands, and Rotational Correlation Times. *Chemistry - A European Journal 8*, 1031–1039.

(30) Aime, S.; Barge, A.; Borel, A.; Botta, M.; Chemerisov, S.; Merbach, A. E.; Müller, U.; Pubanz, D. A Multinuclear NMR Study on the Structure and Dynamics of Lanthanide(III)

Complexes of the Poly(Amino Carboxylate) $EGTA^{4-}$ in Aqueous Solution. *Inorganic Chemistry 36*, 5104–5112.

(31) Baranyai, Z.; Botta, M.; Fekete, M.; Giovenzana, G. B.; Negri, R.; Tei, L.; Platas-Iglesias, C. Lower Ligand Denticity Leading to Improved Thermodynamic and Kinetic Stability of the Gd^{3+} Complex: The Strange Case of OBETA. *Chem. Eur. J.* **2012**, *18* (25), 7680–7685.

(32) Tsien, R. Y. New Calcium Indicators and Buffers with High Selectivity against Magnesium and Protons: Design, Synthesis, and Properties of Prototype Structures. *Biochemistry* **1980**, *19* (11), 2396–2404.

(33) Yuchi, A.; Hirai, M.; Wada, H.; Nakagawa, G. A Novel Stability Sequence of Lanthanoid Complexes with 1,2-Bis(o-Aminophenoxy)Ethane- *N* , *N* , *N* , *N* -Tetraacetic Acid. *Chem. Lett.* **1990**, *19* (5), 773–776.

(34) Avedano, S.; Tei, L.; Lombardi, A.; Giovenzana, G. B.; Aime, S.; Longo, D.; Botta, M. Maximizing the Relaxivity of HSA-Bound Gadolinium Complexes by Simultaneous Optimization of Rotation and Water Exchange. *Chem. Commun.* **2007**, No. 45, 4726.

(35) Tei, L.; Baranyai, Z.; Botta, M.; Piscopo, L.; Aime, S.; Giovenzana, G. B. Synthesis and Solution Thermodynamic Study of Rigidified and Functionalised EGTA Derivatives. *Org. Biomol. Chem.* **2008**, *6* (13), 2361.

(36) Ishiguro, S.; Wada, H.; Ohtaki, H. Solvation and Protonation of 1,10-Phenanthroline in Aqueous Dioxane Solutions. *BCSJ* **1985**, *58* (3), 932–937.

(37) Zekany, L.; Nagypal, I. PSEQUAD: A Comprehensive Program for the Evaluation of Potentiometric and/or Spectrophotometric Equilibrium Data Using Analytical Derivatives. In *Computational Methods for the Determination of Formation Constants*; Leggett, D. J., Ed.; Springer US: Boston, MA, 1985; pp 291–353.

(38) Kanzaki, R.; Umebayashi, Y.; Uemura, K.; Ishiguro, S. Distribution Thermodynamics of 1,10-Phenanthroline in Non-Ionic Surfactant Triton X-100 Micelles. *Phys. Chem. Chem. Phys.* **2001**, *3* (5), 824–828.

(39) Negri, R.; Baranyai, Z.; Tei, L.; Giovenzana, G. B.; Platas-Iglesias, C.; Bényei, A. C.; Bodnár, J.; Vágner, A.; Botta, M. Lower Denticity Leading to Higher Stability: Structural and Solution Studies of Ln(III)–OBETA Complexes. *Inorg. Chem.* **2014**, *53* (23), 12499–12511.

(40) Baranyai, Z.; Pálinkás, Z.; Uggeri, F.; Brücher, E. Equilibrium Studies on the Gd^{3+} , Cu^{2+} and Zn^{2+} Complexes of BOPTA, DTPA and DTPA-BMA Ligands: Kinetics of Metal-Exchange Reactions of $[Gd(BOPTA)]^{2-}$. *Eur. J. Inorg. Chem.* **2010**, *2010* (13), 1948–1956.

(41) Desreux, J. F.; Merciny, E.; Loncin, M. F. Nuclear Magnetic Resonance and Potentiometric Studies of the Protonation Scheme of Two Tetraaza Tetraacetic Macrocycles. *Inorg. Chem.* **1981**, *20* (4), 987–991.

(42) Cacheris, W. P.; Nickle, S. K.; Sherry, A. D. Thermodynamic Study of Lanthanide Complexes of 1,4,7-Triazacyclononane-N,N’,N"-Triacetic Acid and 1,4,7,10-Tetraazacyclododecane-N,N’,N",N’’’-Tetraacetic Acid. *Inorg. Chem.* **1987**, *26* (6), 958–960.

(43) Harris, W. R.; Raymond, K. N.; Weitl, F. L. Ferric Ion Sequestering Agents. 6. The Spectrophotometric and Potentiometric Evaluation of Sulfonated Tricatecholate Ligands. *J. Am. Chem. Soc.* **1981**, *103* (10), 2667–2675.

(44) Manning, T. J.; Gravley, E. D. Protonation Sequence Study of the Solution Structure of DTPA by ^{1}H NMR. *Spectroscopy Letters* **1995**, *28* (3), 291–300.

(45) Rodríguez-Rodríguez, A.; Garda, Z.; Ruscsák, E.; Esteban-Gómez, D.; de Blas, A.; Rodríguez-Blas, T.; Lima, L. M. P.; Beyler, M.; Tripier, R.; Tircsó, G.; Platas-Iglesias, C. Stable Mn^{2+} , Cu^{2+} and Ln^{3+} Complexes with Cyclen-Based Ligands Functionalized with Picolinate Pendant Arms. *Dalton Trans.* **2015**, *44* (11), 5017–5031.

(46) Uzal-Varela, R.; Rodríguez-Rodríguez, A.; Wang, H.; Esteban-Gómez, D.; Brandariz, I.; Gale, E. M.; Caravan, P.; Platas-Iglesias, C. Prediction of Gd(III) Complex Thermodynamic Stability. *Coord. Chem. Rev.* **2022**, 214606.

(47) Sarka, L.; Burai, L.; Brücher, E. The Rates of the Exchange Reactions between [Gd(DTPA)]2− and the Endogenous Ions Cu2+ and Zn2+: A Kinetic Model for the Prediction of the In Vivo Stability of [Gd(DTPA)]2−, Used as a Contrast Agent in Magnetic Resonance Imaging. *Chem. Eur. J.* **2000**, *6* (4), 719–724.

(48) Wang, X.; Jin, T.; Comblin, V.; Lopez-Mut, A.; Merciny, E.; Desreux, J. F. A Kinetic Investigation of the Lanthanide DOTA Chelates. Stability and Rates of Formation and of Dissociation of a Macrocyclic Gadolinium(III) Polyaza Polycarboxylic MRI Contrast Agent. *Inorg. Chem.* **1992**, *31* (6), 1095–1099.

(49) Supkowski, R. M.; Horrocks, W. DeW. On the Determination of the Number of Water Molecules, q, Coordinated to Europium(III) Ions in Solution from Luminescence Decay Lifetimes. *Inorganica Chimica Acta* **2002**, *340*, 44–48.

(50) Armaroli, N.; De Cola, L.; Balzani, V.; Sauvage, J.-P.; Dietrich-Buchecker, C. O.; Kern, J.-M. Absorption and Luminescence Properties of 1, 10-Phenanthroline, 2, 9-Diphenyl-1, 10-Phenanthroline, 2,9-Dianisyl-1, 10-Phenanthroline and Their Protonated Forms in Dichloromethane Solution. *J. Chem. Soc., Faraday Trans.* **1992**, *88* (4), 553.

(51) Binnemans, K. Interpretation of Europium(III) Spectra. *Coordination Chemistry Reviews* **2015**, *295*, 1–45.

(52) Wilkinson, A. J.; Maffeo, D.; Beeby, A.; Foster, C. E.; Williams, J. A. G. Sensitization of Europium(III) Luminescence by Benzophenone-Containing Ligands: Regioisomers, Rearrangements and Chelate Ring Size, and Their Influence on Quantum Yields. *Inorg. Chem.* **2007**, *46* (22), 9438–9449.

(53) Charbonnière, L. J.; Weibel, N.; Retailleau, P.; Ziessel, R. Relationship Between the Ligand Structure and the Luminescent Properties of Water-Soluble Lanthanide Complexes Containing Bis(Bipyridine) Anionic Arms. *Chem. Eur. J.* **2007**, *13* (1), 346–358.

(54) Nielsen, L. G.; Sørensen, T. J. Including and Declaring Structural Fluctuations in the Study of Lanthanide(III) Coordination Chemistry in Solution. *Inorg. Chem.* **2020**, *59* (1), 94–105.

(55) Beeby, A.; Clarkson, I. M.; Dickins, R. S.; Faulkner, S.; Parker, D.; Royle, L.; de Sousa, A. S.; Williams, J. A. G.; Woods, M. Non-Radiative Deactivation of the Excited States of Europium, Terbium and Ytterbium Complexes by Proximate Energy-Matched OH, NH and CH Oscillators: An Improved Luminescence Method for Establishing Solution Hydration States. *J. Chem. Soc., Perkin Trans. 2* **1999**, No. 3, 493–504.

(56) Chauvin, A.; Gumy, F.; Imbert, D.; Bünzli, J. G. Europium and Terbium *Tris*(Dipicolinates) as Secondary Standards for Quantum Yield Determination. *Spectroscopy Letters* **2004**, *37* (5), 517–532.

(57) Petoud, S.; Cohen, S. M.; Bünzli, J.-C. G.; Raymond, K. N. Stable Lanthanide Luminescence Agents Highly Emissive in Aqueous Solution: Multidentate 2-Hydroxyisophthalamide Complexes of Sm^{3+} , Eu^{3+} , Tb^{3+} , Dy^{3+}. *J. Am. Chem. Soc.* **2003**, *125* (44), 13324–13325.

(58) Le Fur, M.; Molnár, E.; Beyler, M.; Fougère, O.; Esteban-Gómez, D.; Rousseaux, O.; Tripier, R.; Tircsó, G.; Platas-Iglesias, C. Expanding the Family of Pyclen-Based Ligands Bearing Pendant Picolinate Arms for Lanthanide Complexation. *Inorg. Chem.* **2018**, *57* (12), 6932–6945.
(59) Esteban-Gómez, D.; de Blas, A.; Rodríguez-Blas, T.; Helm, L.; Platas-Iglesias, C. Hyperfine Coupling Constants on Inner-Sphere Water Molecules of Gd ^{III} -Based MRI Contrast Agents. *ChemPhysChem* **2012**, *13* (16), 3640–3650.
(60) Regueiro-Figueroa, M.; Platas-Iglesias, C. Toward the Prediction of Water Exchange Rates in Magnetic Resonance Imaging Contrast Agents: A Density Functional Theory Study. *J. Phys. Chem. A* **2015**, *119* (24), 6436–6445.
(61) Banerjee, S.; Ghose, M.; Paul, S. S.; Patra, S.; Mukherjea, K. K. A Gadolinium(III) Complex: Synthesis, Structure, Photophysical Profile and Its Role in the Degradation of Nitroaromatics. *Journal of Coordination Chemistry* **2016**, *69* (4), 604–617.
(62) Porcar-Tost, O.; Olivares, J. A.; Pallier, A.; Esteban-Gómez, D.; Illa, O.; Platas-Iglesias, C.; Tóth, É.; Ortuño, R. M. Gadolinium Complexes of Highly Rigid, Open-Chain Ligands Containing a Cyclobutane Ring in the Backbone: Decreasing Ligand Denticity Might Enhance Kinetic Inertness. *Inorg. Chem.* **2019**, *58* (19), 13170–13183.
(63) Raitsimring, A. M.; Astashkin, A. V.; Baute, D.; Goldfarb, D.; Caravan, P. W-Band ^{17} O Pulsed Electron Nuclear Double Resonance Study of Gadolinium Complexes with Water. *J. Phys. Chem. A* **2004**, *108* (35), 7318–7323.
(64) Powell, D. H.; Dhubhghaill, O. M. N.; Pubanz, D.; Helm, L.; Lebedev, Y. S.; Schlaepfer, W.; Merbach, A. E. Structural and Dynamic Parameters Obtained from ^{17} O NMR, EPR, and NMRD Studies of Monomeric and Dimeric Gd $^{3+}$ Complexes of Interest in Magnetic Resonance Imaging: An Integrated and Theoretically Self-Consistent Approach ^{1}. *J. Am. Chem. Soc.* **1996**, *118* (39), 9333–9346.
(65) Laurent, S.; Elst, L. V.; Muller, R. N. Comparative Study of the Physicochemical Properties of Six Clinical Low Molecular Weight Gadolinium Contrast Agents. *Contrast Media Mol Imaging* **2006**, *1* (3), 128–137.
(66) Rohrer, M.; Bauer, H.; Mintorovitch, J.; Requardt, M.; Weinmann, H.-J. Comparison of Magnetic Properties of MRI Contrast Media Solutions at Different Magnetic Field Strengths. *Investigative Radiology* **2005**, *40* (11), 715–724.
(67) Swift, T. J.; Connick, R. E. NMR-Relaxation Mechanisms of O ^{17} in Aqueous Solutions of Paramagnetic Cations and the Lifetime of Water Molecules in the First Coordination Sphere. *The Journal of Chemical Physics* **1962**, *37* (2), 307–320.
(68) Swift, T. J.; Connick, R. E. Erratum: NMR-Relaxation Mechanisms of ^{17} O in Aqueous Solutions of Paramagnetic Cations and the Lifetime of Water Molecules in the First Coordination Sphere. *The Journal of Chemical Physics* **1964**, *41* (8), 2553–2554.
(69) Lammers, H.; Maton, F.; Pubanz, D.; van Laren, M. W.; van Bekkum, H.; Merbach, A. E.; Muller, R. N.; Peters, J. A. Structures and Dynamics of Lanthanide(III) Complexes of Sugar-Based DTPA-Bis(Amides) in Aqueous Solution: A Multinuclear NMR Study. *Inorg. Chem.* **1997**, *36* (12), 2527–2538.
(70) Caravan, P.; Esteban-Gómez, D.; Rodríguez-Rodríguez, A.; Platas-Iglesias, C. Water Exchange in Lanthanide Complexes for MRI Applications. Lessons Learned over the Last 25 Years. *Dalton Trans.* **2019**, *48* (30), 11161–11180.
(71) Nizou, G.; Molnár, E.; Hamon, N.; Kálmán, F. K.; Fougère, O.; Rousseaux, O.; Esteban-Gòmez, D.; Platas-Iglesias, C.; Beyler, M.; Tircsó, G.; Tripier, R. Pyclen-Based Ligands

Bearing Pendant Picolinate Arms for Gadolinium Complexation. *Inorg. Chem.* **2021**, *60* (4), 2390–2405.

(72) Rodríguez-Rodríguez, A.; Esteban-Gómez, D.; de Blas, A.; Rodríguez-Blas, T.; Fekete, M.; Botta, M.; Tripier, R.; Platas-Iglesias, C. Lanthanide(III) Complexes with Ligands Derived from a Cyclen Framework Containing Pyridinecarboxylate Pendants. The Effect of Steric Hindrance on the Hydration Number. *Inorg. Chem.* **2012**, *51* (4), 2509–2521.

(73) Pálinkás, Z.; Roca-Sabio, A.; Mato-Iglesias, M.; Esteban-Gómez, D.; Platas-Iglesias, C.; de Blas, A.; Rodríguez-Blas, T.; Tóth, É. Stability, Water Exchange, and Anion Binding Studies on Lanthanide(III) Complexes with a Macrocyclic Ligand Based on 1,7-Diaza-12-Crown-4: Extremely Fast Water Exchange on the Gd^{3+} Complex. *Inorg. Chem.* **2009**, *48* (18), 8878–8889.

(74) Mato-Iglesias, M.; Rodríguez-Blas, T.; Platas-Iglesias, C.; Starck, M.; Kadjane, P.; Ziessel, R.; Charbonnière, L. Solution Structure and Dynamics, Stability, and NIR Emission Properties of Lanthanide Complexes with a Carboxylated Bispyrazolylpyridyl Ligand. *Inorg. Chem.* **2009**, *48* (4), 1507–1518.

(75) Peters, J. A.; Djanashvili, K.; Geraldes, C. F. G. C.; Platas-iglesias, C. Structure, Dynamics, and Computational Studies of Lanthanide-Based Contrast Agents. In *The Chemistry of Contrast Agents in Medical Magnetic Resonance Imaging*; Merbach, A., Helm, L., Tóth, É., Eds.; John Wiley & Sons, Ltd: Chichester, UK, 2013; pp 209–276.

(76) Raya-Barón, Á.; Oña-Burgos, P.; Fernández, I. Diffusion NMR Spectroscopy Applied to Coordination and Organometallic Compounds. In *Annual Reports on NMR Spectroscopy*; Elsevier, 2019; Vol. 98, pp 125–191.

(77) Vander Elst, L.; Sessoye, A.; Laurent, S.; Muller, R. N. Can the Theoretical Fitting of the Proton-Nuclear-Magnetic-Relaxation-Dispersion (Proton NMRD) Curves of Paramagnetic Complexes Be Improved by Independent Measurement of Their Self-Diffusion Coefficients? *Helv. Chim Acta* **2005**, *88* (3), 574–587.

(78) Poh, A. W. J.; Aguilar, J. A.; Kenwright, A. M.; Mason, K.; Parker, D. Aggregation of Rare Earth Coordination Complexes in Solution Studied by Paramagnetic and DOSY NMR. *Chem. Eur. J.* **2018**, *24* (60), 16170–16175.

(79) Irving, H. M.; Miles, M. G.; Pettit, L. D. A Study of Some Problems in Determining the Stoicheiometric Proton Dissociation Constants of Complexes by Potentiometric Titrations Using a Glass Electrode. *Analytica Chimica Acta* **1967**, *38*, 475–488.

(80) Meiboom, S.; Gill, D. Modified Spin-Echo Method for Measuring Nuclear Relaxation Times. *Review of Scientific Instruments* **1958**, *29* (8), 688–691.

(81) Raiford, D. S.; Fisk, C. L.; Becker, E. D. Calibration of Methanol and Ethylene Glycol Nuclear Magnetic Resonance Thermometers. *Anal. Chem.* **1979**, *51* (12), 2050–2051.

(82) Carr, H. Y.; Purcell, E. M. Effects of Diffusion on Free Precession in Nuclear Magnetic Resonance Experiments. *Phys. Rev.* **1954**, *94* (3), 630–638.

(83) Johnson, C. S. Diffusion Ordered Nuclear Magnetic Resonance Spectroscopy: Principles and Applications. *Progress in Nuclear Magnetic Resonance Spectroscopy* **1999**, *34* (3–4), 203–256.

(84) Mills, R. Self-Diffusion in Normal and Heavy Water in the Range 1-45.Deg. *J. Phys. Chem.* **1973**, *77* (5), 685–688.

(85) Cohen, Y.; Avram, L.; Frish, L. Diffusion NMR Spectroscopy in Supramolecular and Combinatorial Chemistry: An Old Parameter?New Insights. *Angew. Chem. Int. Ed.* **2005**, *44* (4), 520–554.

(86) Does, M. D.; Juttukonda, M. R.; Dortch, R. D. MERA Toolbox (1D,2D Multi-Exponential Relaxation Analysis).
(87) Frisch, M. J.; Trucks, G. W.; Schlegel, H. B.; Scuseria, G. E.; Robb, M. A.; Cheeseman, J. R.; Scalmani, G.; Barone, V.; Mennucci, B.; Petersson, G. A.; Nakatsuji, H.; Caricato, M.; Li, X.; Hratchian, H. P.; Izmaylov, A. F.; Bloino, J.; Zheng, G.; Sonnenberg, J. L.; Hada, M.; Ehara, M.; Toyota, K.; Fukuda, R.; Hasegawa, J.; Ishida, M.; Nakajima, T.; Honda, Y.; Kitao, O.; Nakai, H.; Vreven, T.; Montgomery Jr., J. A.; Peralta, J. E.; Ogliaro, F.; Bearpark, M. J.; Heyd, J.; Brothers, E. N.; Kudin, K. N.; Staroverov, V. N.; Kobayashi, R.; Normand, J.; Raghavachari, K.; Rendell, A. P.; Burant, J. C.; Iyengar, S. S.; Tomasi, J.; Cossi, M.; Rega, N.; Millam, N. J.; Klene, M.; Knox, J. E.; Cross, J. B.; Bakken, V.; Adamo, C.; Jaramillo, J.; Gomperts, R.; Stratmann, R. E.; Yazyev, O.; Austin, A. J.; Cammi, R.; Pomelli, C.; Ochterski, J. W.; Martin, R. L.; Morokuma, K.; Zakrzewski, V. G.; Voth, G. A.; Salvador, P.; Dannenberg, J. J.; Dapprich, S.; Daniels, A. D.; Farkas, Ö.; Foresman, J. B.; Ortiz, J. V.; Cioslowski, J.; Fox, D. J. Gaussian 09, Gaussian, Inc.: Wallingford, CT, USA, 2009. .
(88) Tao, J.; Perdew, J. P.; Staroverov, V. N.; Scuseria, G. E. Climbing the Density Functional Ladder: Nonempirical Meta–Generalized Gradient Approximation Designed for Molecules and Solids. *Phys. Rev. Lett.* **2003**, *91* (14), 146401.
(89) Staroverov, V. N.; Scuseria, G. E.; Tao, J.; Perdew, J. P. Comparative Assessment of a New Nonempirical Density Functional: Molecules and Hydrogen-Bonded Complexes. *The Journal of Chemical Physics* **2003**, *119* (23), 12129–12137.
(90) Dolg, M.; Stoll, H.; Savin, A.; Preuss, H. Energy-Adjusted Pseudopotentials for the Rare Earth Elements. *Theoret. Chim. Acta* **1989**, *75* (3), 173–194.
(91) Andrae, D.; Häußermann, U.; Dolg, M.; Stoll, H.; Preuß, H. Energy-Adjustedab Initio Pseudopotentials for the Second and Third Row Transition Elements. *Theoret. Chim. Acta* **1990**, *77* (2), 123–141.
(92) Tomasi, J.; Mennucci, B.; Cammi, R. Quantum Mechanical Continuum Solvation Models. *Chem. Rev.* **2005**, *105* (8), 2999–3094.
(93) Neese, F. The ORCA Program System. *WIREs Comput Mol Sci* **2012**, *2* (1), 73–78.
(94) Aravena, D.; Neese, F.; Pantazis, D. A. Improved Segmented All-Electron Relativistically Contracted Basis Sets for the Lanthanides. *J. Chem. Theory Comput.* **2016**, *12* (3), 1148–1156.
(95) Weigend, F.; Ahlrichs, R. Balanced Basis Sets of Split Valence, Triple Zeta Valence and Quadruple Zeta Valence Quality for H to Rn: Design and Assessment of Accuracy. *Phys. Chem. Chem. Phys.* **2005**, *7* (18), 3297.
(96) Pantazis, D. A.; Chen, X.-Y.; Landis, C. R.; Neese, F. All-Electron Scalar Relativistic Basis Sets for Third-Row Transition Metal Atoms. *J. Chem. Theory Comput.* **2008**, *4* (6), 908–919.
(97) Neese, F.; Wennmohs, F.; Hansen, A.; Becker, U. Efficient, Approximate and Parallel Hartree–Fock and Hybrid DFT Calculations. A 'Chain-of-Spheres' Algorithm for the Hartree–Fock Exchange. *Chemical Physics* **2009**, *356* (1–3), 98–109.
(98) Izsák, R.; Neese, F. An Overlap Fitted Chain of Spheres Exchange Method. *The Journal of Chemical Physics* **2011**, *135* (14), 144105.
(99) Stoychev, G. L.; Auer, A. A.; Neese, F. Automatic Generation of Auxiliary Basis Sets. *J. Chem. Theory Comput.* **2017**, *13* (2), 554–562.

SYNOPSIS

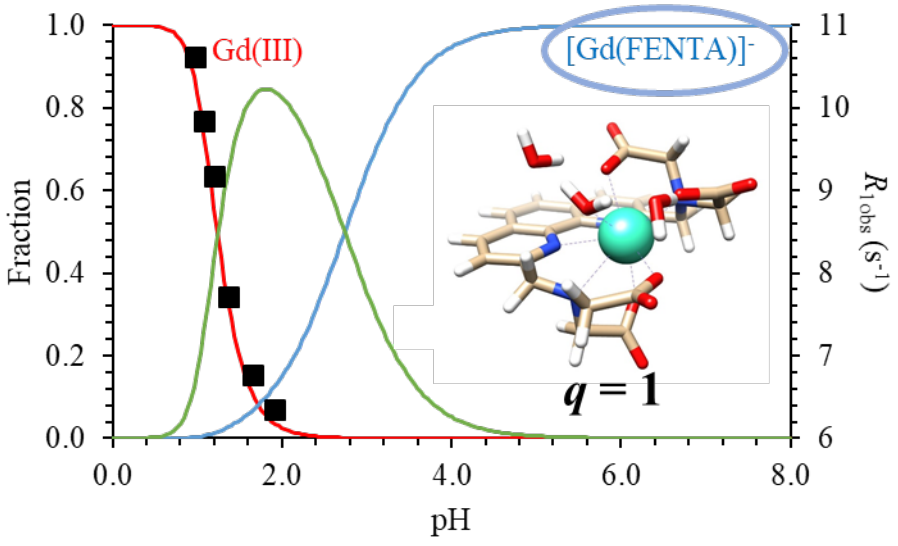

The thermodynamic, kinetic, relaxation and structural features of the Gd(III) complex of a phenanthroline-based ligand (H_4FENTA) have been investigated in detail and compared to the clinically used $[Gd(DTPA)]^{2-}$ and $[Gd(DOTA)]^{-}$. The results show that the $[Gd(FENTA)]^{-}$ possesses similar stability to those of the DTPA and DOTA complexes, dissociates 4 times slower than $[Gd(DTPA)]^{2-}$ and its relaxivity values are almost one unit higher than those of the reference chelates.